Dalton Transactions

Accepted Manuscript

ROYAL SOCIETY OF CHEMISTRY

www.rsc.org/dalton

A Theoretical Study on Tuning Electronic Structures and Photophysical Properties of New Designed Platinum(II) Complexes by Adding Substituents on Functionalized Ligands as Highly Efficient OLED emitters

Luqiong Zhang, Li Tian, Ming Li, Rongxing He, Wei Shen*

By imitating FIrpic, seven new platinum(II) complexes with pic (pic=picolinate) ligand have been designed to be guest materials by means of adding different substituents on functionalized ligands (ppy and fpy, ppy=phenylpyridyl-N,C and fpy=2-(9', 9'-diethyl-9H-fluorenyl)pyridyl-N,C). In order to reveal their molecular structures, photophysical properties and structure-property relationships with typical host materials, an in-depth theoretical investigation was elaborated via quantum chemical calculations. The electronic structures and photophysical properties of these complexes were investigated by density functional theory (DFT) and time-dependent density functional theory (TDDFT) using B3LYP function with LANL2DZ and 6-31G* basis sets. It turns out that electronic structures and photophysical properties can be tuned by substituent modifications on functionalized ligands. This work highlights that a match between guest materials and host materials in typical OLED structures can be weighed by energy levels of HOMO and LUMO and adiabatic triplet energy of each complex. Also a combined analysis among electronic structures, host-guest match, reorganization energies (λ) and triplet exciton generation fraction (χ_T) is favorable to explore triplet emitters with high phosphorescence efficiency in OLEDs, which is an interesting and creative aspect in this work. Thereinto, λ reveals the ability of carrier transport and the balance between holes and electrons, whilst structural parameters and d-orbital splittings show that those complexes with strong electron-withdrawing and electron-donating groups were nonemissive. Consequently, **3**-**7** complexes can be better triplet emitters than FIrpic. Moreover, the emission colors could be predicted by 0-0 transition energy (E_{0-0}) instead of the triplet vertical transition energy (E_{vert}). Accordingly, complexes **3**, **4** and **6** would be efficiently phosphorescent materials with different predicted emission colors.

1 Introduction

Organic light-emitting diodes (OLEDs) and other electroluminescent devices based on phosphorescent transition metal complexes have aroused wide attentions[1, 2]. As for a particular application, the effectiveness of a transition metal complex lies in its electronic excited states, which can be modified optimally by various types of coordinating ligands and metal ions, such as Ir (□)[3-9], Pt(II)[4, 10-15] and Pd(II)[10, 14] etc. In most cases, OLEDs doped with organometallic compounds can achieve higher quantum efficiencies[16-19] with strong spin-orbit coupling (SOC) that get singlet-triplet excited states mixed sufficiently[20]. Among these organometallic phosphors, Pt(II) complexes tend to form planar molecular geometries due to a d^8-electron configuration of Pt(II) ion. And they have several different highly emissive excited states, that is, ligand-to-ligand charge transfer (LLCT) excited states[21], metal-to-ligand charge transfer (MLCT) excited states[22], oligomeric metal-metal-to-ligand charge transfer (MMLCT) excited states[23] and monomer metal-centered d-d excited states (dd*)[24]. Accordingly, some significant intermolecular interactions could be observed in fluid or solid states which are discussed through relevant photophysical properties and electronic structures[25-29].

School of Chemistry and Chemical Engineering, Southwest University, Chongqing, 400715, China, E-mail: shenw@swu.edu.cn Fax: +86-23-68254602;

†Electronic Supplementary information (ESI) available: Details on calculated trans- or cis-configuration of complex **1**, a energy match in OLED, molecular orbital compositions, stimulated absorption spectra and optimised coordinates of complexes **1**-**7** at their respective optimised S_0 and T_1 geometries.

Furthermore, systematic ligand modifications could bring about many alterations over the corresponding excited-state properties and emissive characteristics, like high phosphorescence quantum yield, tunable emission energy, high color purity and good balance between hole and electron. Thus Pt(II) complexes have become popular to be doped into the next generation of OLEDs with full-color performances[30] and white light-emitting OLEDs (WOLEDs)[31-34]. Then for cyclometalated complexes, what are their emission colors in highly efficient OLEDs? How can the emission colors be tuned? The colors electrophosphorescent dopants emit are mostly determined by chelated ligands, chromophoric ligands, ancillary ligands and substituents on these ligands. It has been proved that ligand modifications can dominate emission colors covering the whole visible region (ranging from blue to red)[35]. What's more, those complexes involving large π-conjugated ligands, like 2-phenylpyridyl anion (ppy^-), have superiority that their emission colors can be tuned through adding electron-withdrawing and electron-donating substituents into ppy or chelating ligands[3, 7, 11, 16-19]. As a result, ppy being a typical functionalized ligand is still utilized as the chelating ligand in this paper.

For tuning emission colors, new design strategies in OLED using functional 2–phenylpyridine-type (ppy-type) cyclometalated complexes have been systematically reviewed by Zhou etc. in 2011[36]. Thereinto, a strategy developed by Wong and co-workers[37, 38] showed that the unique color tuning was obtained via introducing the π-accepting $-B(Mes)_2$ group ($B(Mes)_2$=dimesitylboryl) and inductively electron-accepting $-POPh_2$ and $-SO_2Ph$ into ppy. It is because these replacements could shift the origin of MLCT as well as stabilize MLCT states. Apart

from this, other endeavor done by Zachary M Hudson[39] has illustrated triarylboron on ppy ligand could enhance electron injection/electron transport (EI/ET) properties as well as phosphorescence efficiency. These enhancements result from the stabilization of radical anions by boron atom of Lewis acidity, sothat Pt(II) complexes with triarylboron are promising candidates in electrophosphorescent devices. In consideration of this point, -$B(Mes)_2$ is added to the functionalized ligand in this work. Besides，an electron-deficient ring system[40] is also adopted. The electron-deficient ring would be prone to stabilizing the MLCT states and leading a bathochromic shift, so it is an effective tactic to tune emission colors of Pt(II) phosphors. Moreover, the third strategy implemented in this paper is to introduce two ethyl groups and diphenylamine moiety (-NPh_2) into the 9'-position and 2'-position of fluorenylpyridyl (fpy), respectively. This method is in favor of promoting the phosphorescent efficiency as well as color purity[36-41]. Hence, it is judicious to design Pt-complexes with the above-mentioned groups that could tune emission colors and obtain high color purity in OLEDs.

In addition, this work makes a distinct difference from the previous ones[36-41] in that the ancillary ligand has been carried out as pic group unlike acetylacetonate (acac) group in (4,6-dFppy)Pt(acac)[12, 42]. The reasons why we choose pic as an ancillary ligand are attributed to two aspects. One is that several nonborylated N^C-chelate Pt(II) compounds with pic ligand have been applied as phosphorescent dopants in OLEDs, like $(4,6\text{-dFppy})_2$Ir(pic) (FIrpic)[43, 44] ; and another is that pic ligand possesses a higher ligand field strength than that of acac ligand. Herein, the platinum(II) complexes we designed include (ppy)Pt(pic) [**1**; ppy= phenylpyridyl-N,C], (4, 6-dFppy)Pt(pic) [**2**; dFppy=2-(4',6'-difluorophenyl)pyridyl-N, C], $B(Mes)_2$Pt(pic) [**3**; $B(Mes)_2$=2-(4'-dimesitylborylphenyl)pyridyl-N,C], (NPh_2)Pt(pic) [**4**; NPh_2=[(2-4'-diphenylaminophenyl)pyridyl-N,C)], (fpy)Pt(pic) [**5**; fpy=2-(9', 9'-diethyl-9H-fluorenyl)pyridyl-N,C], (NPh_2fpy)Pt(pic) [**6**; NPh_2fpy=9,9-diethyl-N,N-diphenyl-7-(pyridin-2-yl)-9H-fluoren-2-amine-N,C], (fCO)Pt(pic) [**7**; fCO=2-(9H-fluoren-9-onate)pyridyl-N,C] in Figure 1. But all these complexes have trans- and cis- geometries (trans-: the same ligand, pyridyl group, is on the adjacent position in the planar configuration of Pt complexes; cis-: the same ligand located in diagonal position). Because the trans-Pt complexes own lower energies of the S_0 geometries than that of the cis-ones, like (ppy)Pt(pic) shown in Figure S1 and Table S1, we give a top priority to analyzing and discussing the trans-ones. And in this paper these Pt complexes are classified into two groups: ppy-type and fpy-type. **1-4** belong to the ppy-type that phenylpyridyl (ppy) is chromophoric ligand and substituents are situated on the 4'-position of ppy; while **5-7** are the fpy-type with fluorenylpyridyl (fpy) and replacements lie on the 9'-position and 2'-position of fpy.

In order to gain a deep insight into the mechanism of tuning emission colors, DFT and TDDFT have been employed to investigate the electronic effects of different ligands and replacements at the ground state and the excited states[18, 45-53]. Most useful parameters have been computed to analyze the properties of **1-7**, which are compared with FIrpic, the typical phosphorescent triplet emitters in OLEDs. Concerning FIrpic, its theoretically estimated color assessed by adiabatic triplet transition energy (E_T)[54-56] is in good agreement with the realistic emission color. As a result, it is available for the designed complexes to judge their emission colors by E_T. It could be proved clearly that emission colors of complexes **1-7** can be tuned by adding different substituents on the chelated ligands; meanwhile their phosphorescence efficiencies could be enhanced with the increasing ability of electron-withdrawing group or electron-donating group.

Finally, for the sake of better exploring the phosphorescence efficiency, d-orbital splittings and E_T have demonstrated the phosphorescent efficiency-structure relations effectively. Also the comparison of molecular energies and E_T between guest materials and guest materials is an effective and viable approach to measure the phosphorescence efficiency[53-55]. So is the balance between hole transport and electron transport. Sothat, the combined analysis among electronic structures, host-guest match, λ and triplet exciton generation fraction (χ_T) is favorable to weigh whether triplet emitters have high phosphorescence efficiency in OLEDs or not. Overall, this work is of much interest and creativity to exploit the relationship between electronic structures and photophysical properties as well as the phosphorescent efficiency-structure relation.

2 Theoretical Methodology

All the calculations were implemented in the Gaussian09 packages[57]. The ground state (S_0), singlet excited state and the lowest triplet excited state (T_1) geometrical structures of the designed cyclometalated Pt(II) complexes were fully optimized by B3LYP[58] of unrestricted DFT and TDDFT[59], respectively. 6-31G* basis set was for the light atoms (C, H, O, N, F, B) while LANL2DZ basis sets was adopted for Pt atom[60]. The compositions of main molecular orbitals of **1-7** complexes have been analyzed by GaussSum[57] and Aomix[61] programs comprehensively. The electron densities of all molecular orbitals were estimated with code Multiwfn 2.1[62], which would offer detailed descriptions of absorption process. To further understand the photophysical (excitation/emission) properties of this work, we analyzed the natural transition orbitals (NTOs)[63].

Also the reorganization energy (λ) is used to characterize the carrier transport properties of these complexes. λ contains the internal reorganization (λ_{in}) and the out reorganization energy (λ_{in}), namely, $\lambda=\lambda_{in}+\lambda_{out}$. But yet the carrier transferring process takes place in crystals or in amorphous films, which contributes to a smaller λ_{out} and even to be negligible. Therefore, λ_{in} is significant to λ. Aiming at getting a better insight into λ and the transport procedure of hole and electron, the energy barrier for hole injection and electron injection is estimated by the ionization potentials (IPs) and the

electronic affinities (EAs), respectively. The IPs and EAs both are obtained from vertical (v, at the geometry of the neutral molecule) IP and adiabatic (a, optimized structures for both the neutral and charged molecule) EA. Then the hole extraction potentials and the electron extraction potentials are viewed as HEP and EEP, respectively. According to the above-mentioned description, the efficient charge transfer depends mostly upon the value of λ calculated by the following equations[64]:

$$\begin{aligned}\lambda_{hole} &= \lambda_0 + \lambda_+ \\ &= [E^+(M) - E^+(M^+)] + [E(M^+) - E(M)] \\ &= [E^+(M) - E(M)] - [E^+(M^+) - E(M^+)] \\ &= IP(v) - HEP \end{aligned} \quad (1)$$

$$\begin{aligned}\lambda_{electron} &= \lambda_0 + \lambda_- \\ &= [E^-(M) - E^-(M^-)] + [E(M^-) - E(M)] \\ &= [E^-(M) - E^-(M^-)] - [E(M) - E^-(M)] \\ &= EEP - EA(v) \end{aligned} \quad (2)$$

where E, E^+, and E^- represent the energies of the neutral, cation and anion, respectively, while M, M^+, M^- are the geometries of the corresponding neutral, cation and anion. Besides, λ_{hole} and $\lambda_{electron}$ represent the relevant hole reorganization energy and electron reorganization energy. And the difference between λ_{hole} and $\lambda_{electron}$ stands for charge balance, where the variation gets small there is a good balance between hole and electron.

3 Results and Discussion

3.1 Electronic structures at the optimized S_0 and T_1 geometries

3.1.1 Optimized geometries

The corresponding structural parameters of these complexes at both S_0 and T_1 are shown in Table 1 while the schematic structures are presented in Figure 1. The selected bonds including Pt-N_{ppy}, Pt-C_{ppy}, Pt-N_{pic} and Pt-O_{pic} are listed in Table 1. The results show that all the bond lengths get shortened from S_0 state to T_1 state and these variations in complexes **2**-**7** are smaller than complex **1.** The largest variation of Pt-C_{ppy} in complex **1** is 0.046 Å, while the differences of bond lengths of **2**-**7** are less than 0.020 Å. In addition, the variation of dihedral angle □N_{ppy}-C_{ppy}-N_{pic}-O_{pic} from S_0 to T_1 for each complex is 1.984, 0.944, 1.191, 0.033, 0.822, 0.430, 0.289°, successively. From the calculated results, it shows that complexes **1**, **2**, **3** and **5** undergo more remarkable structure changes and amongst the variation of **1** is the most pronounced one. According to the energy-gap law[65], it declares the larger the structural distortion is, the faster the non-radiative rate (κ_{nr}) becomes. Then **1** is more likely to have large non-radiative transfer. The structural distortions between S_0 and T_1 are shown in Figure S2.

3.1.2 Frontier Molecular Orbitals

It is known that the electronic absorption and luminescent properties are affected by geometric optimizations and molecular orbitals, so the analysis of the frontier molecular orbitals (FMOs) has been carried out by DFT method in this work. The frontier molecular orbits plots are illustrated in Figure 2.

First and foremost, the electron densities of HOMOs are almost mainly localized on the phenyl group of ppy, Pt atom and the two oxygen atoms of pic ligand, while the LUMOs are almost mainly situated on the pyridine group of the ppy and pic ligand. The charge distributions of $HOMO_{-m}$ or $LUMO_{+n}$ vary from different substituents to substituents that are situated on ppy or fpy ligand. It is worth noting that there are some remarkable alterations among HOMOs and LUMOs. As for complexes **4** and **6**, the electron densities of HOMOs primarily lie in the phenyl group of ppy and $-NPh_2$ which is a strong electron-donating group. On the other hand, the electron density of LUMOs of complexes **3** resides in the phenyl group of ppy and -$B(Mes)_2$, a strong π-accepting group, linked to ppy, while the HOMO density of complex **7** is delocalized on fpy due to –CO, a weaker electron-withdrawing group. As a result, the substituents effect have a significant influence on the energy levels of HOMOs and LUMOs, that is, the HOMO-LUMO gap (E_g) of each complex is influenced by different substituents. With strong π-accepting group (-$B(Mes)_2$) or strong electron-donating group (-NPh_2) complexes **3**, **4** and **6** have smaller energy gaps than that of the rest ones. The order of E_g in all complexes is **2**(3.79 eV) > **1**(3.65 eV)> **5**(3.45 eV) > **7**(3.44 eV) > **3**(3.41 eV) > **4**(3.18 eV) > **6**(2.94 eV). Seeing from Figure 2, it can be seen evidently that when adding F atoms, -$B(Mes)_2$ and –CO the electron transition characteristics from HOMO to LUMO most are MLCT, LLCT and ILCT, while LLCT and ILCT take place in complexes with strong electron-donating groups. Yet $HOMO_{-1}$, $HOMO_{-2}$ and $HOMO_{-3}$ of **4** and **6** show more compositions of Pt so that it is about to have stronger MCLT from $HOMO_{-n}$ to $LUMO_{+m}$. The more the composition of d-orbital of Pt atom is, the larger the corresponding SOC is going to be.

In addition, so as to understand the structure-property relationship of host materials and guest materials better, these seven complexes have been compared to the classical cyclometalated iridium (Ⅲ) complexes, FIrpic[43, 44], and the typical host materials, such as BCP[66, 67], CBP[43], mCP[68, 69], OXD-7[70] etc. It is of great significance to facilitate carrier transfer by this match between HOMO and LUMO among relevant compounds in OLEDs, as Figure 3 shown. Other information about this match is drawn in Figure S3 and Figure S4. Two considerations should be taken into account. Firstly, as known, the HOMOs and LUMOs energies of the host materials must be larger than that of guest materials, only in this way can it make electrons or holes transport from the host to the guest effectively. Secondly, the closer the HOMOs/LUMOs energies between host materials and guest materials, the more easily and efficiently the transport of holes/electrons become. From Figure 3, the energy-level of BCP and OXD-7 is from -5.79 eV to -1.28 eV and from -6.08 to -1.82 eV, respectively, whilst the energies of Pt complexes range roughly from -5.93 eV to -1.75 eV. Then it obviously manifests that the designed Pt-complexes are more suitable for the host materials while OXD-7 is the optimal choice for all Pt-complexes.

3.1.3 d-Orbital splittings

For the sake of analyzing the non-radiative transfer rate and assessing the phosphorescent efficiency of each designed complex, d-orbital splittings and d-d* transitions stated by Harmut Yersin[71, 72] are introduced to analyze the relevant non-radiative process. For one thing, as for such a statement, it is desirable to own a large splitting between the occupied d state (denoted d) and the unoccupied one (denoted d*), so that the emission quenching induced by the d-d* excitations can be efficiently avoided and become thermally inaccessible[72, 73]. For another, the formally forbidden transitions S_n-T_m can become allowed by a strong SOC generating from heavy metal ions. This strong SOC between S_n and T_m excited states requires a close energy of these two states, which can be depicted by Δdd_{occ}, the energy difference between the two different highest lying occupied d-orbitals[71, 72]. It has been reasoned that the smaller Δdd_{occ} is, the stronger the SOC is and the faster the radiative decay rate will become; meanwhile a large splitting between the highest occupied and the lowest unoccupied d-orbitals, Δdd*, may cause thermally inaccessible metal-centered (MC) d-d excited states[72, 73]. Because the potential-energy minima of a low-lying MC dd excited states displaces distinctively from S_0, it is interesting to interpret the non-emissive behavior of a cyclometalated compound and the relevant nonradiative decay paths by Δdd_{occ} and Δdd*.

The calculated Δdd_{occ} and Δdd* of **1**-**7** at both S_0 and T_1 optimized geometries are presented in Table 2 whilst the frontier molecular orbital compositions of several fragments for 1-7 are listed in Table S3-S9. For Δdd_{occ} the values are evaluated to be 0.62 vs 0.57(**1**), 0.53 vs 0.44 (**2**), 0.61 vs 0.50 (**3**), 0.54 vs 0.25 (**4**), 0.48 vs 0.35 (**5**), 0.55 vs 0.45 (**6**) and 0.53 vs 0.35(**7**) eV at S_0 and T_1, respectively. Judging from the differences of Δdd_{occ} between S_0 and $T_{1,opt}$, there would be stronger SOC and faster radiative decay rate among complexes **2**-**7** which are replaced by different substituents. On the other side, the Δdd* values of **1**-**7** are 5.52, 5.55, 5.48, 5.64, 5.39, 5.46 and 5.29 eV orderly at S_0, all are smaller than that at T_1. Thereinto, the Δdd^* variation between S_0 and $T_{1,opt}$ of complex **2** is the smallest at 0.06 eV, which indicates that other complexes have undergone important structural distortions from S_0 to $T_{1,opt}$ with larger values of Δdd^* and that other complexes may cause remarkable geometric relaxations. That is to say, other complexes may have less access to thermally inaccessible dd* states which have d-d* transition thermally difficult. In addition to the previous discussion about Δdd_{occ}, complexes **3**-**7** have smaller Δdd_{occ} at $T_{1,opt}$, and larger Δdd* between S_0 and $T_{1,opt}$, so they would be expected to own weaker non-radiation process and higher efficiencies in phosphorescence.

3.2 Electronic Absorption spectra

Simulated absorption spectra of **1**-**7** are drawn in Figure 4. Comparing to complex **1**, its derivatives **3**-**7** almost get red-shifted except **2**. These shifts are ascribed to the existences of different substituents which also contribute great to intense transitions for **2**-**7** complexes. The transition behaviors between S_0 and the low-lying singlet excited states (S_n) have been summarized in Table 3, including transition energies, excited energies, oscillator strengths (f), main configurations and the corresponding absorption bands. In this part only the leading excited states of relatively larger intensities have been displayed in this part. And the relevant detailed information about molecular orbitals of **1**-**7** complexes is listed in Table S3-S9, respectively. Seeing from Table S3-S9, the differences in UV-vis absorption spectra are determined by changes of MO energy levels which are induced by the insertion of the above-mentioned substituents in the 4-position of ppy or the 9-position of fpy. Besides, the particular absorption properties are shown in Table S10-S16, which involve transitions from S_0-S_1 to S_0-S_{10} and S_0-S_i (S_i: the strongest excited state).

In Table 3, it reveals clearly that for all complexes the first S_0-S_1 transition characteristic mostly lies in the HOMO-LUMO transition and the corresponding absorption bands are orderly 426.2, 406.2, 451.3, 456.1, 441.6, 479.5 and 450.3 nm orderly. In terms of complexes **1**, **2**, **3**, **5** and **7,** there is a mixed charge transfer characteristic which contains MLCT, LLCT and ILCT in this transition, while **4** and **6** possess a mixed charge transfer of LLCT and ILCT. Because -NPh_2 is a strong electron-donating group which reduces the composition of d orbitals of Pt in HOMOs, MLCT hardly takes place in S_0-S_1 transition for complexes **4** and **6**. However, this kind of transition characteristic still exists in other transitions, like S_0-S_{10} for **4** and S_0-S_{14} for **6**. Besides, detailed contributions to the strongest transitions of absorption spectra should draw great attention to, sothat the electron movements transferring from the ground state to certain excited sates have been illustrated in Figure 5.

The hyacinthine area represents the donor fragment while the navy-blue area is the acceptor one. In this part, only transition contribution over 10.0% of S_0-S_1 and S_0-S_i transitions are taken into account. The S_0-S_1 transitions of all complexes are primarily attributed to the electron densities from HOMO to LUMO, whilst the strongest transitions contain diverse electron transition modes being a mixture of $HOMO_{-m}$ and $LUMO_{+n}$. Most importantly, for complex **3** the strong π-accepting group $-B(Mes)_2$ has shifted the origin of MLCT and stabilized the MLCT excited states; by contrast, complexes **4** and **6** show intense ILCT and LLCT with the introduction of $-NPh_2$. All these particular visualized images of the corresponding transition and some important information have been given to throw light upon the relevant main transition and transition characteristics. The outcomes in Figure 5 are similar to Table 3. Overall, whether introducing the strong π-accepting groups or the strong electron-donating group into functionalized ligand, both they will facilitate to intense transition in absorption spectra.

3.3 Triplet Excited States and Emission Properties

As for typical OLEDs, generally speaking, there may exist three mechanisms causing guest emission in host-guest systems[74, 75]: (1) the singlet excitons forming in the host move to guest via Förster and Dexter energy transfer and then convert to triplet excitons by efficient intersystem crossing (ISC); (2) the triplet excitons forming in the host transfer to guest through Dexter

energy transfer and undergo radiative decay; (3) the holes and electrons coming from the anode and cathode recombine on the phosphorescent guest-materials in EML, triplet excitons generated by charge trapping release to the ground state with phosphorescence emission. On the purpose of exploring the host-guest transfer process and the effective ISC process, the triplet energy match and the triplet exciton generation fractions (χ_T) and have been calculated systematically, respectively.

3.3.1. Adiabatic Triplet Energies

In order to understand the host-guest transfer, the adiabatic triplet energy (E_T) between host and guest is recognized as an ideal criterion to measure the host-guest transfer which is beneficial to holes and electrons transport as well as triplet exactions forming. With regards to the host materials the calculated E_T of OXD-7[70] and BCP[66, 67] are consistent with experimental values, like 2.63 eV vs 2.70 eV[70] and 2.62 eV vs 2.50 eV[66, 67], respectively, seeing Table 4. In other words, our computed results are accessible and valid to a computational extent. And the E_T values of **1**-**7** are 2.52, 2.64, 2.21, 2.28, 2.25, 2.13 and 2.05 eV in sequence. The comparison between host materials and guest materials displays that the E_T values of complexes **3**-**7** are lower than that of the typical host materials, OXD-7 and BCP. It is because of the lower E_T values of guest materials that it would be possible to suppress back-transfer from the guest to the host effectively and that holes and electrons are able to transport from host to guest faster. Most importantly, this effective transport could cause more triplet excitons and highly efficient phosphorescence. Therefore, the designed complexes **3**-**7** could be better guest materials that are suitable to host materials, like OXD-7, in OLEDs. Similarly, the host-guest relation also has been proved in 3.1.2 section.

3.3.2 Triplet exciton generation fraction (χ_T)

On the basis of host-guest transfer, triplet exciton generation fraction (χ_T) is adopted to characterize the ISC process. Being phosphorescent dopants in OLEDs triplet emitters, to have a higher χ_T approaching unity may bring about a maximum ISC rate. It is well-accepted that the faster the ISC is, the higher the probability of phosphorescence is to become. Herein, the triplet exciton generation fractions (χ_T) of (ppy)Pt(pic) and its derivatives were calculated according to the following equation (3)[76]:

$$\chi_T = 3\sigma_T / (\sigma_S + 3\sigma_T) = 3/(\sigma_S/\sigma_T + 3) \qquad (3)$$

In E.q.(3) σ_S and σ_T stand for the formation cross sections of singlet and triplet excitons, respectively. The proportion of σ_S/σ_T is defined as $R_{S/T}$, as follows:

$$R_{S/T} = \sigma_S / \sigma_T = (E_g - E_{S0-Tm}) / (E_g - E_{S0-Sn}) \qquad (4)$$

where E_g is defined as the energy gap between HOMO and LUMO, while E_{S0-Sn} and E_{S0-Tm} are excitation energies from the ground state (S_0) to the *n*th excited singlet state (S_n) and the *m*th excited triplet state (T_m), respectively. In other words, $R_{S/T}$ is the energy ratio between the coupling S_n and the emitting T_m. According to the Kasha rule, it usually defaults *n* and *m* as 1 and the calculated $R_{S/T}$ values and other information have been listed in Table 5. The ratio $R_{S/T}$ is of proportion to $1/\chi_T$, so that $R_{S/T}$ decreases with the increasing of χ_T. For these complexes, the $R_{S/T}$ ratio varies from 0.37 to 0.54 whilst the χ_T ranges from 89.01% to 84.78%. And complexes **3**-**7** practically have a top priority to produce more triplet excitons due to the adding groups on the functionalized groups. As comparing to $(ppy)_2$Irpic and FIrpic, each of the designed Platinum(II) complexes also has an advantage with a higher value of χ_T, that is, the χ_T values of Ir (Ⅲ) complexes and Pt(II) complexes are around 81.0% and over 84.7%, respectively. Due to the higher χ_T, all Pt(II) compounds are prone to generating more triplet exciton and causing faster ISC process. So it is not difficult to say these compounds with higher probabilities of ISC will undergo phosphorescence efficiently.

3.3.3 Natural Triplet Orbitals (NTOs)

Although there is an analysis about the triplet excitons generation, the properties of triplet excited states also need to be noted sothat NTOs are introduced to describe the transition characteristics from $T_{1,opt}$ to S_0[63], as shown in Figure 6. The electron delocalization takes place in ppy and fpy ligands on going from hole-NTO to electron-NTO. And it can be seen evidently that d-orbitals of platinum(II) atom in these complexes contribute directly to ^{3}MLCT which are conductive to having stronger SOC and then make phosphorescence available and efficient in OLEDs. Additionally, the NTOs with highest eigenvalues (λ_i) close to 1 are competent for showing the nature characters of the present electron transition in systems. The results in Figure 6 reveal that complexes **1**, **3,** **4**, **6** and **7** possess relatively higher eigenvalues which are 0.982, 0.996, 0.989, 0.980 and 0.982 orderly, and that the value of **3** is the largest and the second largest is **4**. In summary, there primarily occur ^{3}MLCT and ^{3}ILCT excited states for all complexes, thereinto, **3**, **4** and **7** could be thought as the better candidates for being the phosphorescent organometallic compounds in OLEDs.

3.3.4 Transition Energy and Predictive Emission Color

It is well-known that two kinds of triplet transition energies, the 0-0 transition energy and the adiabatic triplet energy, could be used to depict emission properties of cyclometalated complexes. The 0-0 transition energy allow for the zero-point energies (zpe) of both S_0 and $T_{1,opt}$ at their respective optimized geometries, which actually is the adiabatic triplet energy (E_T). The vertical transition energy is the electronic-energy difference between the $T_{1,opt}$ and S_0 states at the $T_{1,opt}$ optimized geometries[24], which is achieved by the ΔSCF method, seeing ESI. These two transition energies are listed in Table 4. Ascribed to the substituent effects, complexes **2**-**7** have different transition energies while **1** and **2** have the similar values to $(ppy)_2$Ir(pic) and FIrpic, respectively. Being a typical blue phosphorescent material, FIrpic, the calculated outcome is in accordance with the experimental one, where the 0-0transition energy can be used to predict the relevant emission color theoretically.

Near the end of our work, Wang and co-workers[77]

have synthesized complex **3** and done some experimental and theoretical research about its photophysical properties. The outcome revealed that complex **3** emitted green which was in good line with our theoretical result. It is Wang's work that proved we could predict the colors of triplet emitters by E_T. Then according to E_T, the emission colors of these complexes can be forecast as sky-blue, brilliant blue, dark green, bright green, bright green, yellow and amber, successively, in Table 4. Based on the above calculated results, it can be seen that the adding substituents probably bring about pronouncedly different charge transfer characters as well as different emission colors, particularly in complexes **3**-**7**.

3.4 Charge Transportation Properties

Good charge mobility and charge balance are determined by hole/electron injection and reorganization energy (λ), respectively. To the best of our knowledge, the value of ionization potential (IP) is smaller, the hole injection is much easier; on the other side, the electron affinity (EA) value is larger, the electron injection is easier. And λ is accustomed to evaluating the charge transfer rate and the balance between hole and electron. It is worth noting that λ_{hole} values decrease and $\lambda_{electron}$ ones increase as introducing these substituents. And the values of λ_{hole} and $\lambda_{electron}$ have been calculated whilst the energy barriers for the injection of holes and electrons are estimated by ionization potentials (IPs) and electron affinities (EAs), respectively. All these values are implemented by Eq.2 and Eq.3 based on the Marcus theory[78-80], as listed in Table 6. As for the hole/electron injection, complexes **3**-**7** are overall superior to the initial Pt(II) complex **1**, since they have relatively smaller IPs and larger EAs. Apart from this, we also make an analysis about the π-accepting ability and electron-donating ability of substituent groups. Thereinto, the order of the ability of π-accepting groups is $–F < –C=O < –B(Mes)_2$, sothat for complexes with these groups the order of λ_{hole} is **7** > **3** > **2** and the $\lambda_{electron}$ order is **7** < **2** < **3**. On the other hand, the order of electron-donating ability is $–(CH_2CH_3)_2 <–NPh_2$, then for complexes **4**-**6** the order of λ_{hole} and $\lambda_{electron}$ are **5** > **4** > **6** and **5** < **4** < **6**, respectively. The stronger the π-accepting or the electron-donating ability is, the smaller λ_{hole} is, and the larger $\lambda_{electron}$ is. For all Pt(II) complexes, finally, the differences Δλ between λ_{hole} and $\lambda_{electron}$ are in the sequence of 0.224, 0.193, 0.079, -0.060, 0.067, -0.047 and 0.043 eV, which illustrates that **3**-**7** are the better materials in phosphorescent OLEDs with good carrier transfer rate.

4 Conclusions

In this work, geometry optimizations, electronic structures and photophysical properties of these seven platinum(II) complexes were investigated by DFT/TDDFT calculations. Comparing to the frontier molecular orbitals (FMOs), both the levels of $HOMO_{-m}$ and $LUMO_{+n}$ have changed distinctly by introducing $–B(Mes)_2$ and $–NPh_2$ which cause various transition characters for relevant absorption and emissions processes. Regarding the absorption process, there occur strong MLCT, LLCT and ILCT which make great contribution to have intense transitions, these transitions are ascribed to the adding replacements $-B(Mes)_2$ group and $-NPh_2$ group. With the addition of a large steric hindrance effect and electronic effect of these two groups, complexes **3**, **4** and **6** own better geometrical structures with fewer distortions between S_0 and $T_{1,opt}$. Hereinto, a detailed analysis of d-orbital splittings at S_0 and $T_{1,opt}$ optimized geometries provides a support to verify that those compounds with strong π-accepting group and electron-donating group would undergo weaker geometry relaxation than others. Thus, **3**-**7** complexes have faster radiative rate as dd* excitation get weakened.

And the computational rations between singlet and triplet excitons in the excitation process shows that these designed complexes have larger ratios than that of typical complexes FIrpic and $(ppy)_2$Irpic. So the designed complexes are more likely to have stronger SOC as well as highly efficient phosphorescence in the course of emissive excitation. Besides, the combinational discussion of charge transport properties and the host-guest match throws light upon that complexes **3**-**7** have better charge transport ability. Furthermore, based on the 0-0 transition energies, the emission colors have been forecasted, and it has a good agreement with experimental results.

In consideration of all relevant properties, complexes **3**-**7** could be good candidates as phosphorescent dopants in OLEDs with emitting different colors, thereinto complexes **3**, **4** and **6** tune emission colors more notably and may perhaps show higher phosphorescence efficiencies with better carrier transport.

Acknowledgments

This work was supported by National Natural Science Foundation of China (Grant No.21073144), and by Fundamental Research Funds for the Central Universities (Grant No. XDJK2010B009).

References

1. M. Baldo, D. O'brien, Y. You, A. Shoustikov, S. Sibley, M. Thompson and S. Forrest, *nature*, 1998, **395**, 151-154.
2. H. Yersin, *Highly efficient OLEDs with phosphorescent materials*, Wiley. com, 2008.
3. T. Sajoto, P. I. Djurovich, A. Tamayo, M. Yousufuddin, R. Bau, M. E. Thompson, R. J. Holmes and S. R. Forrest, *Inorganic chemistry*, 2005, **44**, 7992-8003.
4. S. Lamansky, R. C. Kwong, M. Nugent, P. I. Djurovich and M. E. Thompson, *Organic Electronics*, 2001, **2**, 53-62.
5. S. Lamansky, P. Djurovich, D. Murphy, F. Abdel-Razzaq, H.-E. Lee, C. Adachi, P. E. Burrows, S. R. Forrest and M. E. Thompson, *Journal of the American Chemical Society*, 2001, **123**, 4304-4312.
6. M. Baldo, S. Lamansky, P. Burrows, M. Thompson and S. Forrest, *Applied Physics Letters*, 1999, **75**, 4.
7. M. Baldo, M. Thompson and S. Forrest, *nature*, 2000, **403**, 750-753.
8. C. Adachi, M. A. Baldo, M. E. Thompson and S. R. Forrest, *Journal of Applied Physics*, 2001, **90**, 5048-5051.
9. L. Yang, F. Okuda, K. Kobayashi, K. Nozaki, Y. Tanabe, Y. Ishii and M.-a. Haga, *Inorganic chemistry*,

2008, **47**, 7154-7165.
10. H. Yersin and D. Donges, in *Transition Metal and Rare Earth Compounds*, Springer, 2001, pp. 81-186.
11. W. Lu, B.-X. Mi, M. C. Chan, Z. Hui, C.-M. Che, N. Zhu and S.-T. Lee, *Journal of the American Chemical Society*, 2004, **126**, 4958-4971.
12. J. Brooks, Y. Babayan, S. Lamansky, P. I. Djurovich, I. Tsyba, R. Bau and M. E. Thompson, *Inorganic chemistry*, 2002, **41**, 3055-3066.
13. V. Adamovich, J. Brooks, A. Tamayo, A. M. Alexander, P. I. Djurovich, B. W. D'Andrade, C. Adachi, S. R. Forrest and M. E. Thompson, *New journal of chemistry*, 2002, **26**, 1171-1178.
14. T. Matsushita, T. Asada and S. Koseki, *The Journal of Physical Chemistry A*, 2006, **110**, 13295-13302.
15. Y. Wu, S.-X. Wu, H.-B. Li, Y. Geng and Z.-M. Su, *Dalton Transactions*, 2011, **40**, 4480-4488.
16. M. K. Nazeeruddin, R. Wegh, Z. Zhou, C. Klein, Q. Wang, F. De Angelis, S. Fantacci and M. Grätzel, *Inorganic chemistry*, 2006, **45**, 9245-9250.
17. H. J. Bolink, E. Coronado, S. G. Santamaria, M. Sessolo, N. Evans, C. Klein, E. Baranoff, K. Kalyanasundaram, M. Graetzel and M. K. Nazeeruddin, *Chemical Communications*, 2007, 3276-3278.
18. I. Avilov, P. Minoofar, J. Cornil and L. De Cola, *Journal of the American Chemical Society*, 2007, **129**, 8247-8258.
19. M. Xu, R. Zhou, G. Wang, Q. Xiao, W. Du and G. Che, *Inorganica Chimica Acta*, 2008, **361**, 2407-2412.
20. M. G. Colombo, A. Hauser and H. U. Guedel, *Inorganic chemistry*, 1993, **32**, 3088-3092.
21. D. A. Vezzu, J. C. Deaton, J. S. Jones, L. Bartolotti, C. F. Harris, A. P. Marchetti, M. Kondakova, R. D. Pike and S. Huo, *Inorganic chemistry*, 2010, **49**, 5107-5119.
22. S.-Y. Chang, J. Kavitha, S.-W. Li, C.-S. Hsu, Y. Chi, Y.-S. Yeh, P.-T. Chou, G.-H. Lee, A. J. Carty and Y.-T. Tao, *Inorganic chemistry*, 2006, **45**, 137-146.
23. S.-W. Lai and C.-M. Che, in *Transition Metal and Rare Earth Compounds*, Springer, 2004, pp. 27-63.
24. G. S. M. Tong and C. M. Che, *Chemistry-A European Journal*, 2009, **15**, 7225-7237.
25. T. J. Wadas, Q.-M. Wang, Y.-j. Kim, C. Flaschenreim, T. N. Blanton and R. Eisenberg, *Journal of the American Chemical Society*, 2004, **126**, 16841-16849.
26. Y. Y. Scaffidi-Domianello, A. A. Nazarov, M. Haukka, M. Galanski, B. K. Keppler, J. Schneider, P. Du, R. Eisenberg and V. Y. Kukushkin, *Inorganic chemistry*, 2007, **46**, 4469-4482.
27. S. C. Kui, S. S.-Y. Chui, C.-M. Che and N. Zhu, *Journal of the American Chemical Society*, 2006, **128**, 8297-8309.
28. J. Moussa, K. M.-C. Wong, L.-M. Chamoreau, H. Amouri and V. W.-W. Yam, *Dalton Transactions*, 2007, 3526-3530.
29. W. Lu, M. C. Chan, N. Zhu, C.-M. Che, C. Li and Z. Hui, *Journal of the American Chemical Society*, 2004, **126**, 7639-7651.
30. T. Jüstel, H. Nikol and C. Ronda, *Angewandte Chemie International Edition*, 1998, **37**, 3084-3103.
31. J. Kido, M. Kimura and K. Nagai, *Science*, 1995, **267**, 1332-1334.
32. B. W. D'Andrade and S. R. Forrest, *Advanced Materials*, 2004, **16**, 1585-1595.
33. Z. H. Kafafi, *Organic electroluminescence*, CRC Press, 2005.
34. B. D'Andrade, *Nature Photonics*, 2007, **1**, 33-34.
35. Y. You and S. Y. Park, *Journal of the American Chemical Society*, 2005, **127**, 12438-12439.
36. G. Zhou, W. Y. Wong and X. Yang, *Chemistry–An Asian Journal*, 2011, **6**, 1630-1630.
37. G. Zhou, Q. Wang, X. Wang, C.-L. Ho, W.-Y. Wong, D. Ma, L. Wang and Z. Lin, *Journal of Materials Chemistry*, 2010, **20**, 7472-7484.
38. G. Zhou, C. L. Ho, W. Y. Wong, Q. Wang, D. Ma, L. Wang, Z. Lin, T. B. Marder and A. Beeby, *Advanced Functional Materials*, 2008, **18**, 499-511.
39. Z. M. Hudson, C. Sun, M. G. Helander, H. Amarne, Z. H. Lu and S. Wang, *Advanced Functional Materials*, 2010, **20**, 3426-3439.
40. G.-J. Zhou, Q. Wang, W.-Y. Wong, D. Ma, L. Wang and Z. Lin, *Journal of Materials Chemistry*, 2009, **19**, 1872-1883.
41. G.-J. Zhou, X.-Z. Wang, W.-Y. Wong, X.-M. Yu, H.-S. Kwok and Z. Lin, *Journal of organometallic chemistry*, 2007, **692**, 3461-3473.
42. B. Ma, P. I. Djurovich and M. E. Thompson, *Coordination Chemistry Reviews*, 2005, **249**, 1501-1510.
43. C. Adachi, R. C. Kwong, P. Djurovich, V. Adamovich, M. A. Baldo, M. E. Thompson and S. R. Forrest, *Applied Physics Letters*, 2001, **79**, 2082-2084.
44. Y. Kawamura, K. Goushi, J. Brooks, J. J. Brown, H. Sasabe and C. Adachi, *Applied Physics Letters*, 2005, **86**, 071104.
45. K. Nozaki, *JOURNAL-CHINESE CHEMICAL SOCIETY TAIPEI*, 2006, **53**, 101.
46. X. Li, B. Minaev, H. Ågren and H. Tian, *The Journal of Physical Chemistry C*, 2011, **115**, 20724-20731.
47. X. Li, B. Minaev, H. Ågren and H. Tian, *European Journal of Inorganic Chemistry*, 2011, **2011**, 2517-2524.
48. B. Minaev, V. Minaeva and H. Ågren, *The Journal of Physical Chemistry A*, 2009, **113**, 726-735.
49. E. Jansson, B. Minaev, S. Schrader and H. Ågren, *Chemical physics*, 2007, **333**, 157-167.
50. P. J. Hay, *The Journal of Physical Chemistry A*, 2002, **106**, 1634-1641.
51. B. Minaev, H. Ågren and F. D. Angelis, *Chemical physics*, 2009, **358**, 245-257.
52. T. Hofbeck and H. Yersin, *Inorganic chemistry*, 2010, **49**, 9290-9299.
53. H. Yersin, D. Donges, W. Humbs, J. Strasser, R. Sitters and M. Glasbeek, *Inorganic chemistry*, 2002, **41**, 4915-4922.
54. R. Holmes, S. Forrest, Y.-J. Tung, R. Kwong, J. Brown, S. Garon and M. Thompson, *Applied Physics Letters*, 2003, **82**, 2422-2424.
55. S. Tokito, T. Iijima, Y. Suzuri, H. Kita, T. Tsuzuki and F. Sato, *Applied Physics Letters*, 2003, **83**, 569-571.
56. D. Tanaka, Y. Agata, T. Takeda, S. Watanabe and J. Kido, *Japanese Journal of Applied Physics*, 2007, **46**, L117-L119.
57. M. Frisch, G. Trucks, H. Schlegel, G. Scuseria, M. Robb, J. Cheeseman, G. Scalmani, V. Barone, B.

Mennucci and G. Petersson, *Inc.: Wallingford, CT*, 2009, **115**.
58. A. D. Becke, *The Journal of Chemical Physics*, 1993, **98**, 5648.
59. A. D. Becke, *Physical Review A*, 1988, **38**, 3098.
60. P. J. Hay and W. R. Wadt, *The Journal of Chemical Physics*, 1985, **82**, 299.
61. S. I. Gorelsky, 2007.
62. T. Lu.
63. R. L. Martin, *Journal of Chemical Physics*, 2003, **118**, 4775-4777.
64. N. F. Mott and E. A. Davis, *Electronic processes in non-crystalline materials*, Oxford University Press, 2012.
65. J. S. Wilson, N. Chawdhury, M. R. Al-Mandhary, M. Younus, M. S. Khan, P. R. Raithby, A. Köhler and R. H. Friend, *Journal of the American Chemical Society*, 2001, **123**, 9412-9417.
66. P. Strohriegl and J. V. Grazulevicius, *Advanced Materials*, 2002, **14**, 1439-1452.
67. V. I. Adamovich, S. R. Cordero, P. I. Djurovich, A. Tamayo, M. E. Thompson, B. W. D'Andrade and S. R. Forrest, *Organic Electronics*, 2003, **4**, 77-87.
68. S. J. Yeh, M. F. Wu, C. T. Chen, Y. H. Song, Y. Chi, M. H. Ho, S. F. Hsu and C. H. Chen, *Advanced Materials*, 2005, **17**, 285-289.
69. Q. Wang, J. Ding, D. Ma, Y. Cheng, L. Wang and F. Wang, *Advanced Materials*, 2009, **21**, 2397-2401.
70. J. Lee, N. Chopra, S.-H. Eom, Y. Zheng, J. Xue, F. So and J. Shi, *Applied Physics Letters*, 2008, **93**, 123306.
71. A. F. Rausch, H. H. Homeier, P. I. Djurovich, M. E. Thompson and H. Yersin, Proc. of SPIE Vol, 2007.
72. H. Yersin and W. J. Finkenzeller, *Highly Efficient OLEDs with Phosphorescent Materials*, 2008, 1-98.
73. J. G. Williams, in *Photochemistry and Photophysics of Coordination Compounds II*, Springer, 2007, pp. 205-268.
74. Y. Tao, C. Yang and J. Qin, *Chemical Society Reviews*, 2011, **40**, 2943-2970.
75. M. Baldo and S. Forrest, *Physical Review B*, 2000, **62**, 10958.
76. S. Yin, L. Chen, P. Xuan, K.-Q. Chen and Z. Shuai, *The Journal of Physical Chemistry B*, 2004, **108**, 9608-9613.
77. S.-B. Ko, J.-S. Lu, Y. Kang and S. Wang, *Organometallics*, 2013, **32**, 599-608.
78. R. A. Marcus, *The Journal of Chemical Physics*, 1956, **24**, 966-978.
79. R. Marcus, *Annual Review of Physical Chemistry*, 1964, **15**, 155-196.
80. R. A. Marcus, *Reviews of Modern Physics*, 1993, **65**, 599-610.

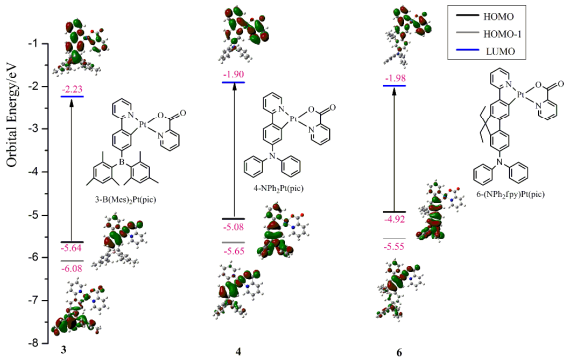

From the energy-level diagrams, it could be obviously seen that the electron transitions from $HOMO_{-m}$ to LUMO are different, which are induced by the different added substituents on functionalised ligands in the designed platinum (II) complexes. When adding strong π-accepting and strong electron-donating groups on functionalised ligands, not only have the energy gaps become smaller but also the characteristics of MLCT could be stabilized. It is because of these alterations that the relevant photophysical properties have been improved.

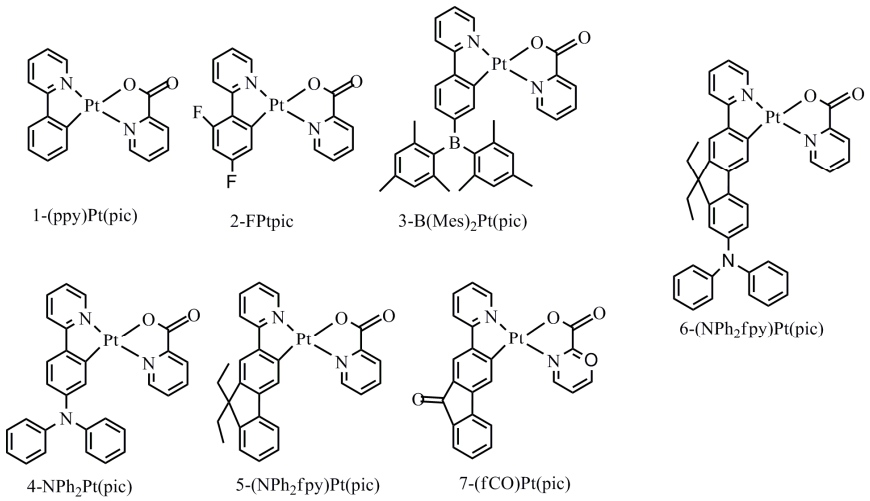

Figure 1 The molecular structures of Cyclometalated platinum(II) complexes

Table 1 Selected bond distances(Å), dihedral angles(°) and dipole moment(D) at both S_0 and T_1 geometries for 1-7, respectively

complexes		Bond length (Å)				Dihedral angles (deg/°)
		Pt-N(ppy)	Pt-C(ppy)	Pt-N(pic)	Pt-O(pic)	Nppy-Cppy-Npic-Opic
1	S_0	2.025	2.017	2.074	2.133	-6.029
	T_1	2.009	1.971	2.077	2.110	-8.014
2	S_0	2.024	2.013	2.077	2.122	6.004
	T_1	2.003	1.979	2.077	2.107	6.948
3	S_0	2.026	2.017	2.076	2.130	5.305
	T_1	2.019	1.972	2.089	2.105	6.496
4	S_0	2.027	2.015	2.074	2.132	5.959
	T_1	2.009	1.997	2.075	2.127	5.926
5	S_0	2.024	2.018	2.075	2.132	6.460
	T_1	2.011	1.987	2.075	2.121	7.282
6	S_0	2.024	2.016	2.073	2.136	-6.473
	T_1	2.012	1.997	2.073	2.133	-6.903
7	S_0	2.025	2.012	2.076	2.126	6.693
	T_1	2.019	1.993	2.072	2.122	6.982

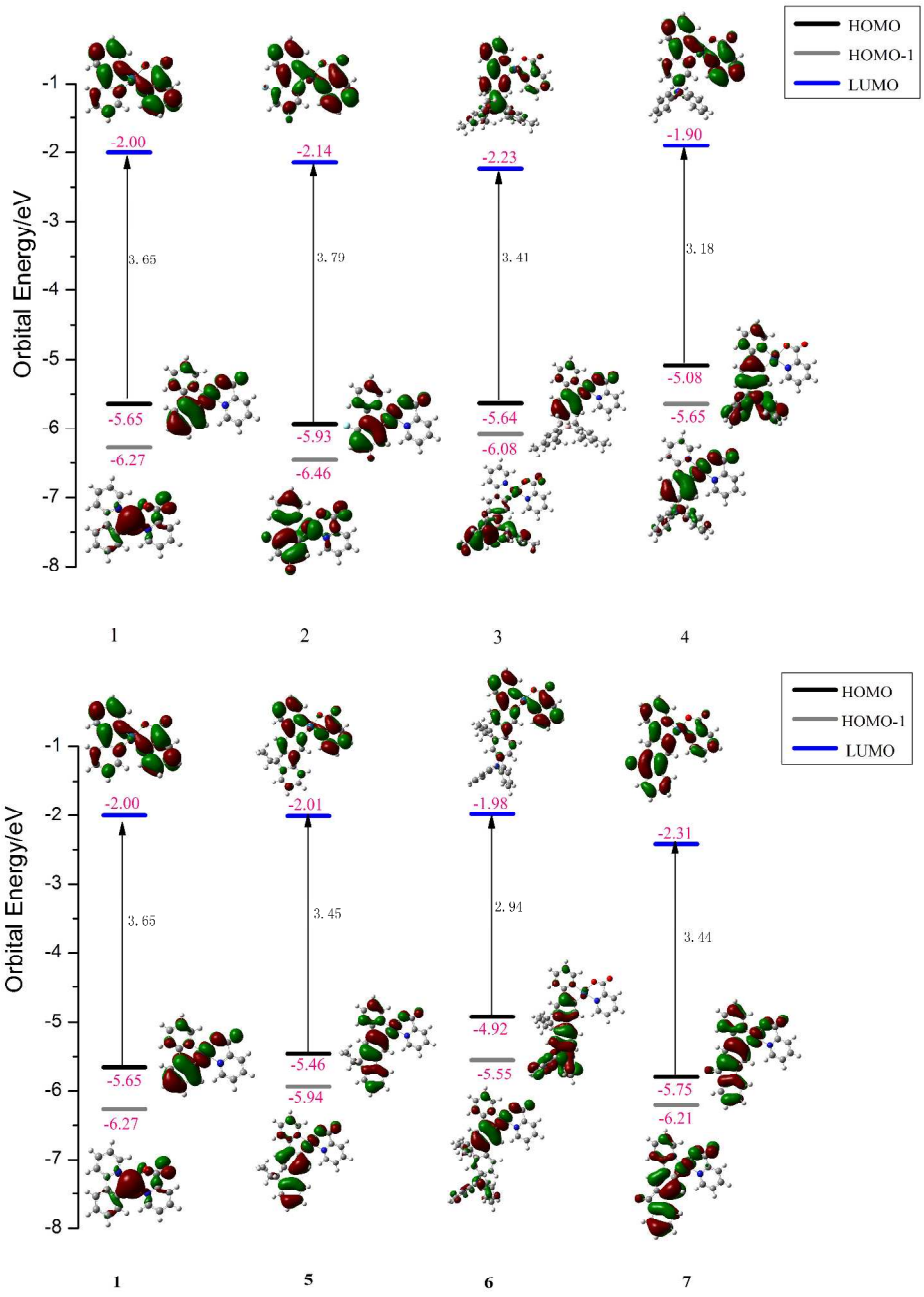

Figure 2 Molecular orbital diagrams, HOMO and LUMO energies for Pt-complexes at their S_0 optimized geometries

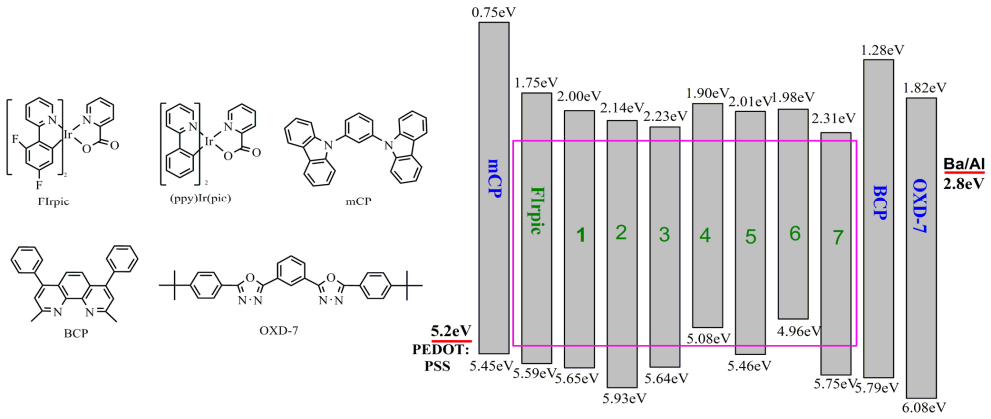

Figure 3 Calculated energy-level diagram and chemical structures of the referenced typical host materials and FIrpic

Table 2 The calculated energies of HOMO, LUMO, energy gap (E_g), transition energy, Δdd_{occ} and Δdd^* (eV) of **1**−**7**.

Complexes	E_{HOMO}	E_{LUMO}	ΔE_g	S_0		$T_{1,opt}$	
				Δdd_{occ}	Δdd^*	Δdd_{occ}	Δdd^*
1	-5.65	-2.00	3.65	0.62	5.52	0.57	5.68
2	-5.93	-2.14	3.79	0.53	5.55	0.44	5.61
3	-5.64	-2.23	3.41	0.61	5.48	0.50	5.75
4	-5.08	-1.90	3.18	0.54	5.64	0.25	5.74
5	-5.46	-2.01	3.45	0.48	5.39	0.35	5.69
6	-4.92	-1.98	2.94	0.55	5.46	0.45	5.85
7	-5.75	-2.31	3.44	0.53	5.29	0.35	5.64
$(ppy)_2Ir(pic)$	-5.17	-1.52	3.65				
FIrpic	-5.59	-1.75	3.84				
BCP	-5.79	-1.28	4.51				
OXD-7	-6.33	-1.82	4.51				

Note: [a]The MO energies are calculated at the gas phase optimized geometries.
[b]Only those with $cd^2 > 0.10$ are given in the table.
[c]"d" refers to the molecular orbitals with dominant d-orbital character, which took the contribution of d (Pt) orbitals over 10% into consideration.

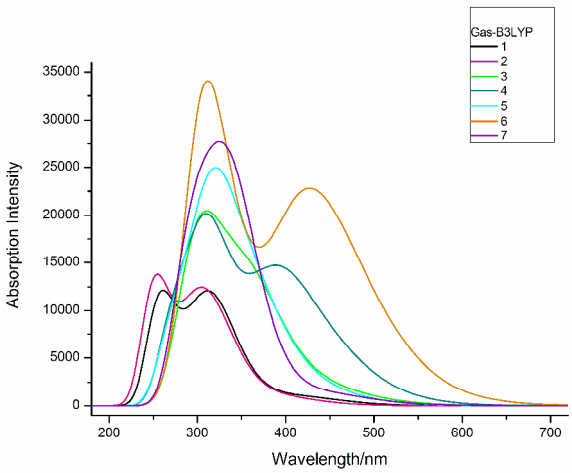

Figure 4 Absorption spectra of the investigated complexes calculated at their optimized S_0 geometry by TDDFT in the gas phase

Table 3 Calculated excited energies, dominant orbital excitation, and oscillator strength(f) from TD-DFT for the designed cyclometalated Pt complexes **1**-**7**.

	λ_{cal} (nm)	f	E_{cal} (eV)	Main configuration			Orbitality interpretation	Character of excitation
				ψi→ψj		Excitation		
1-S_1	426.2	0.019	2.91	81→82	0.699	H→L (98%)	d(Pt)+π(ppy)+π(pic)→π*(ppy)+π*(pic)	MLCT+LLCT+ILCT
S_7	326.5	0.136	3.80	78→82	0.491	H-3→L (48%)	d(Pt)+π(pic)+π(ppy)→π*(ppy)+π*(pic)	MLCT+LLCT+ILCT
S_9	305.2	0.132	4.06	77→82	0.571	H-4→L (65%)	d(Pt)+π(ppy)→π*(ppy)+π*(pic)	MLCT+LLCT+ILCT
S_{25}	256.8	0.156	4.83	78→85	0.450	H-3→L+3 (40%)	d(Pt)+π(pic)+π(ppy)→π*(ppy)+π*(pic)	MLCT+LLCT+ILCT
2-S_1	406.2	0.017	3.05	89→90	0.698	H→L (97%)	π(ppy)+d(Pt)+π(pic)→π*(ppy)+π*(pic)	MLCT+LLCT+ILCT
S_5	329.2	0.106	3.77	88→90	0.537	H-1→L (58%)	π(ppy)+d(Pt)+π(pic)→π*(ppy)+π*(pic)	MLCT+LLCT+ILCT
S_9	300.8	0.105	4.12	89→93	0.535	H→L+3 (57%)	π(ppy)+d(Pt)+π(pic)→π*(ppy)	MLCT+LLCT+ILCT
3-S_1	451.3	0.037	2.75	148→149	0.691	H→L (96%)	d(Pt)+π(ppy)+π(pic)→π*(ppy)+π*(S)	MLCT+LLCT+ILCT
S_5	365.7	0.081	3.39	146→149	0.612	H-2→L (75%)	π(S)→π*(ppy)+π*(S)	LLCT+ILCT
S_7	357.0	0.078	3.47	145→149	0.511	H-3→L (52%)	d(Pt)+π(S)→π*(ppy)+π*(S)	MLCT+LLCT+ILCT
S_{10}	341.3	0.070	3.63	141→149	0.623	H-7→L (78%)	d(Pt)+π(ppy)+π(S)→π*(ppy)+π*(S)	MLCT+LLCT+ILCT
S_{15}	316.3	0.081	3.92	148→152	0.572	H→L+3 (66%)	d(Pt)+π(ppy)+π(pic)→π*(pic)	MLCT+LLCT+ILCT
S_{22}	299.0	0.090	4.15	141→150	0.508	H-7→L+1 (52%)	d(Pt)+π(ppy)+π(S)→π*(pic)	MLCT+LLCT
4-S_1	456.1	0.095	2.72	125→126	0.689	H→L (97%)	π(ppy)+π(S)→π*(ppy)+π*(pic)	LLCT+ILCT
S_3	394.4	0.250	3.14	125→127	0.668	H→L+1 (89%)	π(ppy)+π(S)→π*(ppy)+π*(pic)	LLCT+ILCT
S_{10}	320.9	0.074	3.86	121→126	0.453	H-4→L (41%)	d(Pt)+π(ppy)→π*(ppy)+π*(pic)	MLCT+LLCT+ILCT
				124→128	0.458	H-1→L+2 (42%)	d(Pt)+π(ppy)+π(pic)→π*(ppy)+π*(pic)	
S_{14}	309.7	0.124	4.00	125→131	0.475	H→L+5 (45%)	π(ppy)+π(S)→π*(S)	LLCT+ILCT
5-S_1	441.6	0.032	2.81	120→121	0.680	H→L (92%)	d(Pt)+π(fpy)→π*(fpy)+π*(pic)	MLCT+LLCT+ILCT
S_4	362.8	0.115	3.42	118→121	0.480	H-2→L (46%)	d(Pt)→π*(fpy)+π*(pic)	MLCT+LLCT+ILCT
				119→121	-0.475	H-1→L (45%)	d(Pt)+π(fpy)→π*(fpy)+π*(pic)	
S_9	326.3	0.109	3.80	119→122	0.574	H→L+3 (66%)	d(Pt)+π(fpy)→π*(fpy)+π*(pic)	MLCT+LLCT+ILCT
S_{10}	317.5	0.306	3.91	116→121	0.574	H-4→L (66%)	d(Pt)+π(fpy)→π*(fpy)+π*(pic)	MLCT+LLCT+ILCT
6-S_1	479.5	0.202	2.59	164→165	0.684	H→L (94%)	π(Ph2N-fpy)→π*(pic)+π*(Ph2N-fpy)	LLCT+ILCT
S_3	419.9	0.351	2.95	164→166	0.688	H→L+1 (95%)	π(Ph2N-fpy)→π*(pic)+π*(Ph2N-fpy)	LLCT+ILCT
S_{14}	317.0	0.158	3.91	159→16	0.532	H-5→L (57%)	d(Pt)+π(Ph_2N-fpy)→π*(pic)+π*(Ph_2N-fpy)	MLCT+LLCT+ILCT
S_{15}	309.8	0.188	4.00	164→17	0.561	H→L+5 (63%)	π(Ph2N-fpy)→π*(Ph2N-fpy)	ILCT
S_{16}	306.4	0.181	4.05	162→166	0.510	H-2→L+1 (52%)	π(Ph2N-fpy)→π*(pic)+π*(Ph2N-fpy)	LLCT+ILCT
7-S_1	450.3	0.027	2.75	107→108	0.694	H→L (96%)	d(Pt)+π(CO-fpy)→π*(CO-fpy)	MLCT+ILCT
	347.1	0.345	3.57	106→108	0.427	H-1→L (36%)	d(Pt)+π(CO-ppy)+π(pic)→π*(CO-fpy)	
S_7				107→110	0.352	H→L+2 (25%)	d(Pt)+π(CO-fpy)→π*(pic)+π*(CO-fpy)	MLCT+LLCT+ILCT
				106→109	0.393	H-1→L+1 (27%)	d(Pt)+π(CO-ppy)+π(pic)→π*(pic)+π*(CO-fpy)	
S_{11}	322.7	0.118	3.84	106→109	0.393	H-1→L+1 (31%)	d(Pt)+π(CO-ppy)+π(pic)→π*(pic)+π*(CO-fpy)	MLCT+LLCT+ILCT
				107→111	0.399	H→L+3 (32%)	d(Pt)+π(CO-fpy)→π*(pic)+π*(CO-fpy)	
	293.8	0.149	4.22	101→108	0.383	H-6→L (29%)	π(pic)+π(CO-fpy)→π*(CO-fpy)	
S_{20}				102→109	0.278	H-5→L+1 (15%)	d(Pt)+π(CO-fpy)→π*(pic)+π*(CO-fpy)	LLCT+ILCT+MLCT
				106→111	0.228	H-1→L+3 (10%)	d(Pt)+π(CO-ppy)+π(pic)→π*(pic)+π*(CO-fpy)	

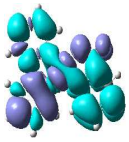

S_0-S_1: $\Phi \approx 0.699\psi_{H\rightarrow L}$
λ=426.2nm f=0.019
Main Transitions: H→L (98%)

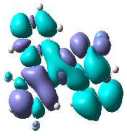

S_0-S_1: $\Phi \approx 0.698\psi_{H\rightarrow L}$
λ=406.2nm f=0.017
Main Transitions: H→L(97%)

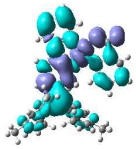

S_0-S_1: $\Phi \approx 0.691\psi_{H\rightarrow L}$
λ=451.3nm f=0.037
Main Transitions: H→L(96%)

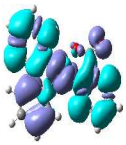

S_0-S_{25}: $\Phi \approx 0.262\psi_{H-4\rightarrow L+1} + 0.450\psi_{H-3\rightarrow L+3}$
λ=256.8nm f=0.156
Main Transitions:
H-4→L+1(14%), H-3→L+3(40%)

1

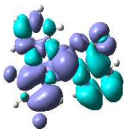

S_0-S_5:$\Phi \approx 0.395\psi_{H-2\rightarrow L} + 0.537\psi_{H-1\rightarrow L}$
λ=329.2nm f=0.106
Main Transitions:
H-2→L(31%), H-1→L(58%)

2

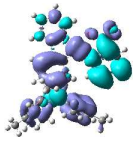

S_0-S_{22}: $\Phi \approx 0.265\psi_{H-8\rightarrow L} + 0.508\psi_{H-7\rightarrow L}$
λ=299.0nm f=0.090
Main Transitions:
H-8->L+1 (14%),H-7->L+1 (52%)

3

S_0-S_1: $\Phi \approx 0.689\psi_{H\rightarrow L}$
λ=456.1nm f=0.095
Main Transitions: H→L(97%)

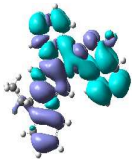

S_0-S_1: $\Phi \approx 0.680\psi_{H\rightarrow L}$
λ=441.6nm f=0.032
Main Transitions: H→L(92%)

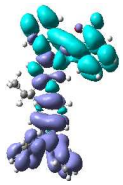

S_0-S_1: $\Phi \approx 0.684\psi_{H\rightarrow L}$
λ=479.5nm f=0.202
Main Transitions: H→L(94%)

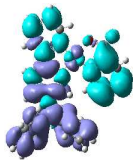

S_0-S_3: $\Phi \approx 0.668\psi_{H\rightarrow L}$
λ=394.4nm f=0.250
Main Transitions: HOMO->L+1 (89%)

4

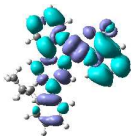

S_0-S_{10}: $\Phi \approx 0.574\psi_{H-4\rightarrow L} + 0.264\psi_{H-1\rightarrow L+1}$
λ=317.5nm f=0.306
Main Transitions:
H-4->L (66%), H-1->L+1 (14%)

5

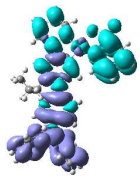

S_0-S_3: $\Phi \approx 0.688\psi_{H\rightarrow L}$
λ=419.9nm f=0.351
Main Transitions: H→L(95%)

6

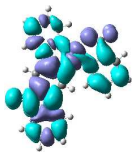

S_0-S_1: $\Phi \approx 0.694\psi_{H\rightarrow L}$
λ=450.3nm f=0.027
Main Transitions: H→L(96%)

7

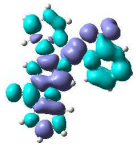

S_0-S_7:$\Phi \approx 0.427\psi_{H-1\rightarrow L} - 0.230\psi_{H-1\rightarrow L+1} + 0.352\psi_{H\rightarrow L+2}$
λ=347.1nm f=0.345
Main Transitions:
H-1->L(36%),H-1->L+1 (11%),H->L+2(25%)

7

Figure 5 Electron Density Difference Plots of Electronic Transitions

Table 4 The calculated triplet energies and the predicted emission colors of complexes **1**−**7**.

Complexes	$\Delta E_{0\text{-}0}(E_T)$		ΔEver		Predicted Emission Colors
	eV	nm	eV	nm	
1	2.52	491.24	2.23	556.63	sky-blue
2	2.65	467.49	2.35	528.16	brilliant blue
3	2.22	558.76	1.94	638.43	dark green
4	2.29	541.85	2.06	601.63	bright green
5	2.25	549.79	1.97	627.5	bright green
6	2.14	580.16	1.89	655.87	yellow
7	2.06	601.6	1.75	707.88	amber
$(ppy)_2Ir(pic)$	2.52	492.21	2.25	550.4	sky-blue
FIrpic	2.66	466.65	2.36	525.96	brilliant blue
BCP	2.62	472.38	2.16	573.61	brilliant blue
OXD-7	2.63	471.03	2.07	598.98	brilliant blue

Note: [a]The calculations of $\Delta E_{0\text{-}0}(E_T)$ and ΔEver see ref 24 and ESI.

[b]The experimental values of E_T refer to ref 66, ref 67 and ref 70.

Table 5 The energies of MOs and the ratio of triplet excitons calculated by DFT/TDDFT.

Complexes	E_{HOMO}	E_{LUMO}	ΔE_g	$\Delta E_{0\text{-}0}$	ΔE_{ver}	$E_{S0\text{-}S1}$	$E_{S0\text{-}T1}$	$\Delta E_{S1\text{-}T1}$	$E_g\text{-}E_{S0\text{-}S1}$	$E_g\text{-}E_{S0\text{-}T1}$	δ_S/δ_T	χ_T (%)
1	-5.65	-2.00	3.65	2.52	2.23	2.91	2.07	0.83	0.74	1.58	0.47	86.45
2	-5.93	-2.14	3.79	2.65	2.35	3.05	2.19	0.87	0.74	1.60	0.46	86.71
3	-5.64	-2.23	3.41	2.22	1.94	2.75	1.79	0.95	0.66	1.62	0.41	87.97
4	-5.08	-1.90	3.18	2.29	2.06	2.72	1.93	0.78	0.46	1.25	0.37	89.01
5	-5.46	-2.01	3.45	2.25	1.97	2.81	1.82	0.99	0.64	1.63	0.39	88.41
6	-4.92	-1.98	2.94	2.14	1.89	2.59	2.16	0.42	0.35	0.78	0.46	86.83
7	-5.75	-2.31	3.44	2.06	1.75	2.75	2.17	0.59	0.69	1.27	0.54	84.78
$(ppy)_2Ir(pic)$	-5.17	-1.52	3.65	2.52	2.25	2.89	2.57	0.32	0.76	1.08	0.70	81.03
FIrpic	-5.59	-1.75	3.84	2.66	2.36	3.09	2.73	0.37	0.75	1.11	0.67	81.76
BCP	-5.79	-1.28	4.51	2.62	2.16	3.86	2.74	1.12	0.65	1.77	0.37	89.08
OXD-7	-6.33	-1.82	4.51	2.63	2.07	3.91	2.68	1.23	0.60	1.83	0.33	90.14

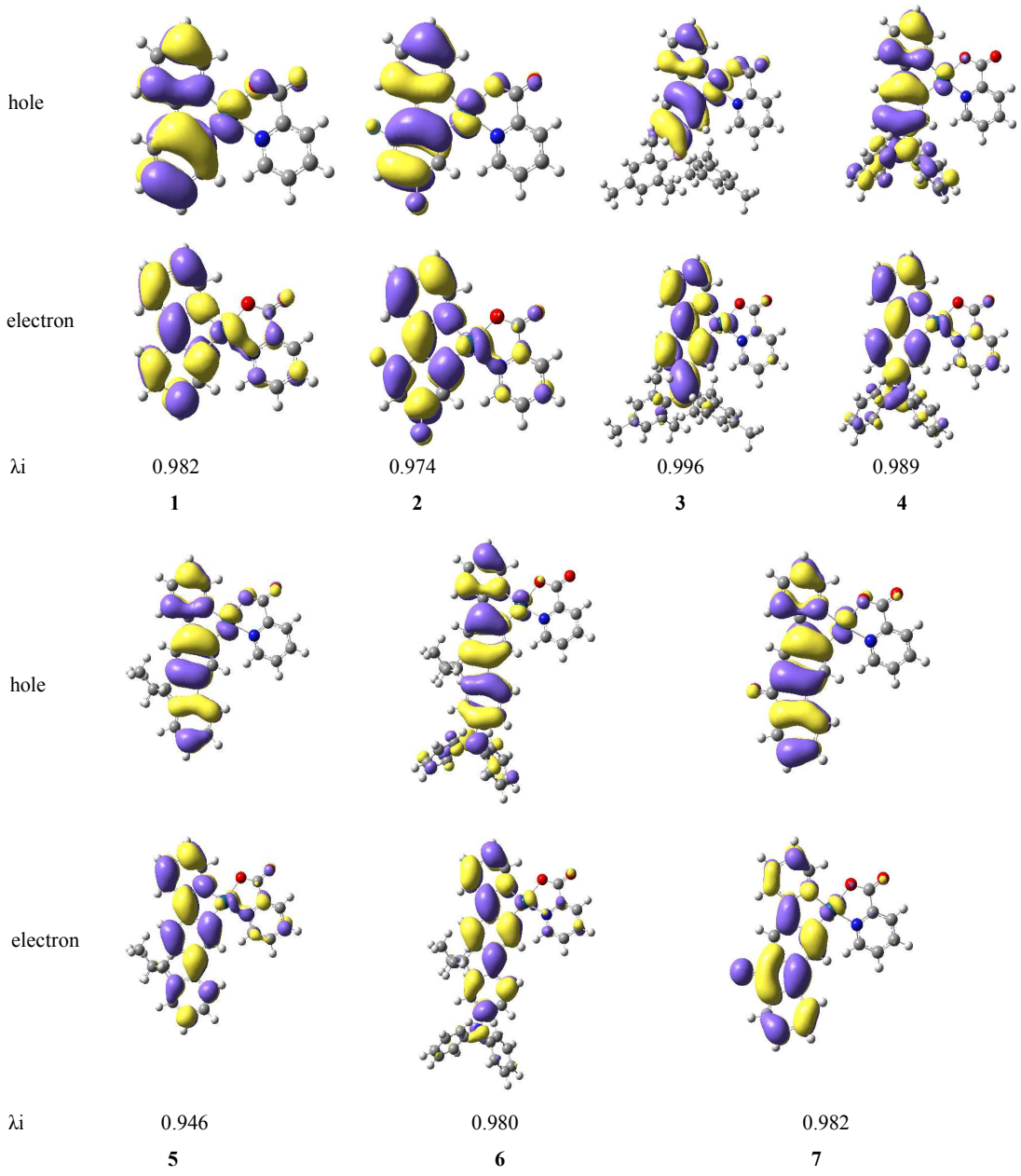

Figure 6 The NTO plots of Pt (Ⅱ) complexes at the lowest triplet excited state ($T_{1,opt.}$)

Table 6 The calculation of the hole/electron reorganization energies (λ) (eV) by DFT.

Complex	IP(v)	IP(a)	HEP	λ_{hole}	EA(v)	EA(a)	EEP	$\lambda_{electron}$	Δλ
1	7.155	6.980	6.737	0.418	0.627	0.723	0.821	0.194	0.224
2	7.427	7.265	7.027	0.400	0.756	0.859	0.964	0.207	0.193
3	6.923	6.771	6.554	0.369	1.093	1.235	1.383	0.290	0.079
4	6.292	6.143	6.066	0.226	0.635	0.778	0.920	0.286	-0.060
5	6.723	6.606	6.481	0.242	0.782	0.869	0.956	0.174	0.067
6	6.014	5.920	5.829	0.185	0.815	0.930	1.047	0.232	-0.047
7	7.091	7.067	6.866	0.225	1.197	1.285	1.379	0.183	0.043